Terrestrial Based Inflatable Dish Antennas

Larry T. Lowe, *Member IEEE*
Phase IV Systems, Inc.
3405 Triana Boulevard
Huntsville, Alabama 35805 USA

Ronald D. Hackett, PE, *Senior Member IEEE*
Paul A. Gierow, PE
SRS Technologies
500 Discovery Drive
Huntsville, AL 35806 USA

Abstract- A terrestrial based 4.8-meter inflatable dish is presented. The dish is constructed using lightweight, thin film technologies used in space-based platforms. A lenticular is formed by seaming two parabolic dish films together. One film is coated with a silver flake conductive paint, the other is RF transparent. The lenticular is inflated to hold the parabolic shape of the dish. The lenticular is attached to the inside of an inflatable spherical radome. The radome provides environmental protection to the thin film lenticular. The lenticular and radome are designed such that the focal point is located on the surface of the radome. An RF feed is attached to the radome at the focal point. The gain of the dish is measured using the sun as an RF source. Solar gain measurement data is presented showing the measured peak gain from the sun and the width of the main beam.

I. INTRODUCTION

For deployable ground-based radar and communication systems, the antenna tends to be the most sensitive element of the system in terms of the electrical and mechanical tradeoffs. Increasing the aperture of an antenna increases the electrical performance, usually expressed as signal-to-noise ratio (SNR), but the increased aperture also results in a heavier system that takes up more volume when stowed. In a deployable system the mechanical constraints of weight and volume limit the size of the antenna. These mechanical constraints can be avoided by taking advantage of space-based antenna technologies [1-4]. High strength, lightweight thin-film polymers have been used for the last decade to create inflatable antennas for space-based platforms. The space-based structures have to be lightweight and stowed in small volumes to be transported into orbit. Applying lightweight, thin-film technologies to ground-based antennas will provide over an order of magnitude reduction in antenna weight and in stowed volume.

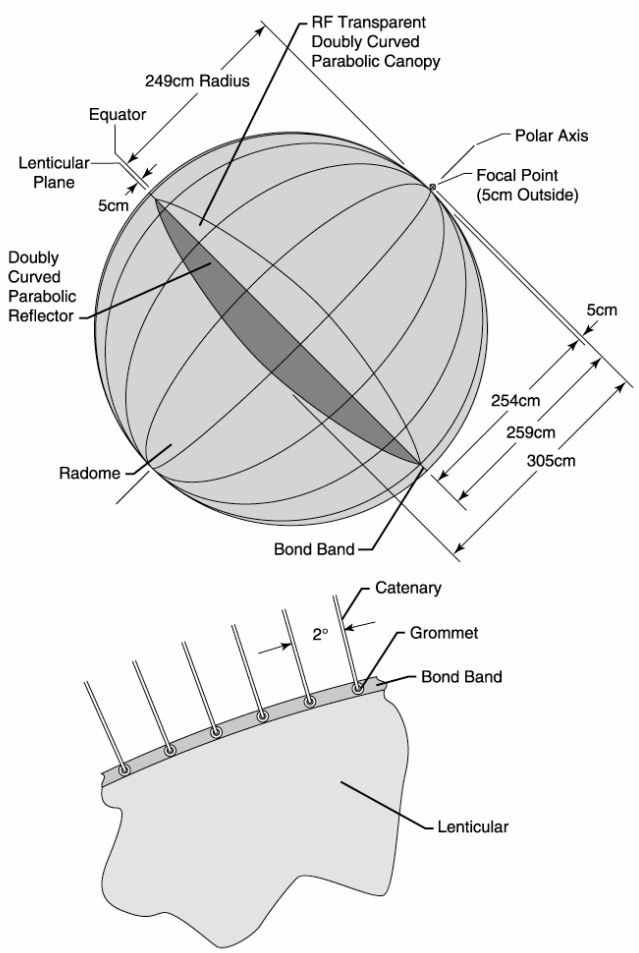

Figure 1. Radome and Lenticular Geometry

SRS Technologies and Phase IV Systems have teamed together and developed a 4.8-meter diameter inflatable dish antenna that demonstrates an increase in aperture size and a reduction in weight, volume, and cost when compared to conventional ground-based dish antennas. The 4.8-meter inflatable dish will be field tested in late March by connecting

Figure 2: Inflatable torus supporting the CP1 lenticular.

it to an existing satellite communication system. The field test will demonstrate the dish in a one-way, receive only data link with an orbiting satellite. A solar gain calibration technique was used to measure the peak gain and antenna pattern of the dish [5-6]. Multiple solar gain measurements were used to place the feed horn to the exact location of the focal point of the dish. The measured gain and beamwidth of the dish match theoretical calculations.

II. Description of Lightweight Inflatable Dish

The antenna reflector is constructed from CP1 polyimide film that is exclusively licensed to SRS Technologies by NASA's Langley Research Center. Two 4.8-meter films are cast and cured on a mandrel with a diameter of 480 cm and a focal length of 305 cm. The films are approximately 25-32 µm thick and are trimmed along the edge to remove anomalies from the casting process. One of the films is coated with a silver flake conductive paint that is applied onto the convex surface of the doubly curved film. The two films are then seamed along the periphery with the two concave surfaces facing each other, as shown in Figure 2. The bond band that is formed by seaming the two films together reduces the aperture of the reflector to 466 cm. An inflation port is added before the peripheral seam is completed. Metal grommets are placed every two degrees around the periphery in the bond band where the two films are joined. Elastic 'springs' connect the grommets with the supporting structure. The tension in the springs is adjusted to remove imperfections in the surface and forms a compliant border. When inflated to the proper pressure, this structure looks like a convex lens and is called the lenticular. The clear CP1 film is called the canopy and the coated CP1 film is called the reflector or concentrator. The initial shape accuracy of the lenticular was measured using a photogrametric technique and was found to have an RMS shape error of 2.67mm at the optimal focal length of 297 cm. The photogrametry test was performed with the collector positioned at a 45 degree angle to include the effects of gravity on the distorted shape. This surface shape accuracy

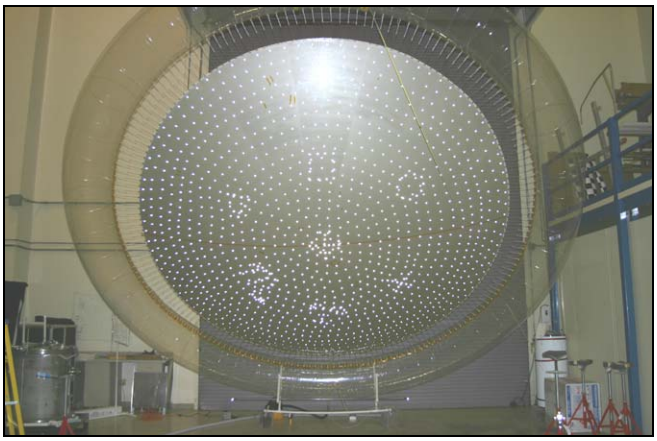

a.

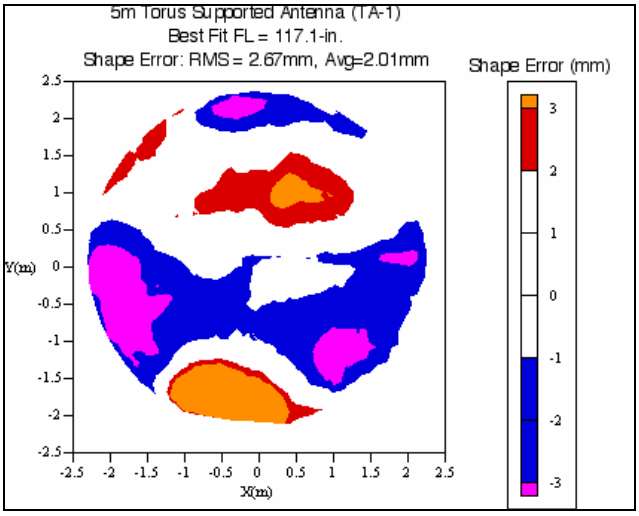

b.

Figure 3: a. Photogrametric Image of the lenticular. b. Reduced photogrametric data.

is within the tolerance for reflector surface roughness reported by Love [7]. Tuning methods have been used to improve the gravity-induced distortion of the collector that was initially measured. An improved shape accuracy of 1-2mm RMS is achievable in practice. The shape accuracy results of the photogrametric process are shown in Figure 3.

The radome is constructed from an RF transparent, flexible and ultraviolet radiation stable material. The geometry for the radome and the lenticular is shown in Figure 1. Eighteen gore sections are cut for each hemisphere to approximate a doubly curved surface. The gore sections are sewn together using heavy duty nylon upholstery thread. The two hemispheres are joined together with a zipper and seal configuration. The diameter of the radome is 498 cm. Clear vinyl windows are installed at strategic locations around the radome to provide visual access to the interior during testing. Plexiglas attachment pads are attached every two degrees around the circle formed by passing a plane through the sphere parallel to the equator and perpendicular to the polar axis of the radome. This plane will coincide with the plane

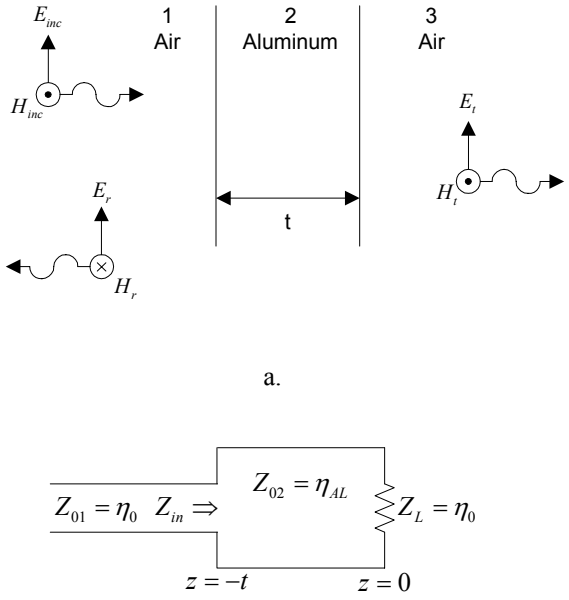

Figure 4. a. Reflection and transmission of incident electric field in an air-Aluminum-air semi-infinite boundary problem. b. Equivalent transmission line model.

defined by the intersection of the canopy and the reflector and is called the plane of the lenticular. The distance from the plane of the lenticular to the focal point is 259 cm. The plane is offset from the equator of the radome by 5 cm so that the focal point is 5 cm outside the radome at one of the poles. This geometry was selected because access to the feed system will be required during testing. When inflated to the proper pressure, the radome provides support for the lenticular and protection from wind and the environment. The compliant borders provide isolation between the radome and the lenticular to dampen movement and distortion caused by the wind. The spherical shape was chosen because it was the optimum shape for the on-axis parabolic reflector and because of its aerodynamic qualities. An analytical model of the spherical radome was developed for a variety of wind velocities. For example, the wind load on the 498 cm radome in a 48 kph wind is 890 Newtons operating through the center of gravity of the sphere. The base and tie-down supports must be designed to counteract this load. The validity of the analytical model and the stability of the radome design has been demonstrated successfully in scale model testing.

The reflectivity of each of the materials used in the lenticular and the radome were measured using a network analyzer. The measurements show that the radome materials and the canopy material of the lenticular are RF transparent, whereas, the Silver coated CP1 reflector is an RF short. The Silver coating on the CP1 material is approximately 200,000 Angstroms thick. This corresponds to about 27 skin depths thick, so it is expected to act, in effect, like an ideal short. A second reflector was constructed with Aluminized mylar.

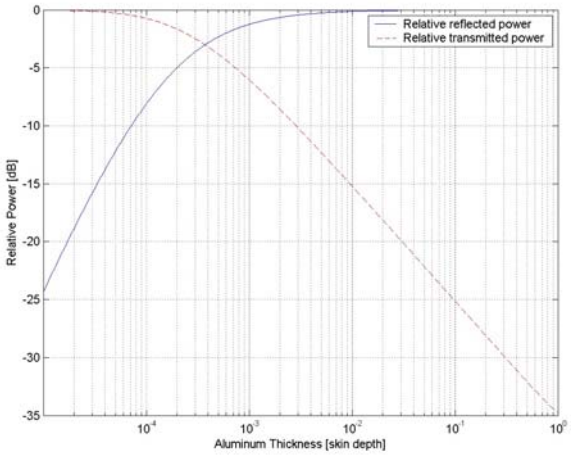

Figure 5. Relative reflected power and relative transmitted power of Aluminum slab as a function of thickness.

The thickness of the Aluminum coating on the second reflector is approximately 1500 Angstroms. This corresponds to about 0.15 skin depths thick. The reflectivity measurement of the network analyzer shows that the Aluminized mylar performs as well as an RF reflector as the Silver coated CP1 material. These measurements indicate that these materials do not have to be multiple skin depths thick in order to be a good RF reflector, which is against the original assumptions of the authors.

An analysis was performed to determine the reflectivity of an Aluminum slab as the thickness is reduced. The problem is modeled as three semi-infinite, contiguous media as shown in Fig. 4. The transmission line equivalent circuit can be used to model the three media as shown in Fig. 4. The lossy transmission line equation can be used to calculate the equivalent input impedance of Aluminum slab in region 2 and the air in region 3. The lossy transmission line equation is expressed as

$$\eta_{IN} = \eta_{AL} \frac{\eta_0 + \eta_{AL} \tanh(\gamma t)}{\eta_{AL} + \eta_0 \tanh(\gamma t)} \tag{1}$$

where $\gamma = \sqrt{j\omega\mu(\sigma + j\omega\varepsilon)}$ is the propagation constant of the Aluminum medium. The reflection coefficient is expressed as

$$\Gamma = \frac{\eta_{IN} - \eta_0}{\eta_{IN} + \eta_0} \tag{2}$$

and the transmission coefficient is related to the reflection coefficient as $\tau = 1 + \Gamma$. The ratio of the power in the reflected wave to the power in the incident wave, which is 1 for a perfect conductor, is calculated as $20 \cdot \log(|\Gamma|)$, and the

insertion loss is expressed as $20 \cdot \log\left(\left|1+\Gamma\right|\right)$. Figure 5 shows a plot of the relative power in the reflective wave and the relative insertion loss as a function of the Aluminum thickness t. The plot in Figure 5 shows that the Aluminum slab is a near perfect reflector at a 0.1 skin depth thickness. The relative reflected power of the 1500 Angstrom (0.15 skin depths) thick Aluminized mylar agree with the plot in Figure 5. The measured predicted data suggest that a conductor does not have to be 5 skin depths in thickness to be a "good" RF reflector. This topic will be explored in greater detail at a later time.

III. Description of RF Feed

In order to reduce the complexity and cost of the initial demonstration, the dish was designed to operate in a receive only mode, thereby eliminating the extra high power transmit amplifier and the waveguide plumming needed to get the high power transmit signal to the feed at the top of the dish. The RF feed structure consists of a pyramidal horn antenna, 90 degree waveguide bend, and a low noise amplifier (LNA). The input to the amplifier is WR-112 waveguide and the output is an SMA connection. The dish is designed to receive a signal in the X_L band from a data communication satellite.

A. Feed Horn Selection

The selection of the optimum feed horn dimensions were calculated by mode matching the feed horn antenna aperture electric filed distribution to the focal plane electric field distribution of the dish. The focal plane electric field of the dish is

$$E_{dish}(\rho) = \frac{2J_1\left(\frac{2\pi a\rho}{\lambda F}\right)}{\left(\frac{2\pi a\rho}{\lambda F}\right)} \tag{3}$$

where a is the radius of the circular dish aperture, F is the focal distance, λ is wavelength, and ρ is the radial distance from the focal point. It is assumed that the phase center of the feed horn is placed at the focal point of the dish.

Waves traveling in unbounded regions have a continuous spectral content, where as waves in bounded regions, such as waveguide, are characterized by discrete spectra. This means that all of the energy in the focal plane electric field distribution of the dish is not going to propagation through the feed horn to the receiver. Due to the limited size of the feed horn aperture, only a fraction of the energy in the dish electric field distribution pattern is present at the aperture of the horn, and only a fraction of the spectral energy in the

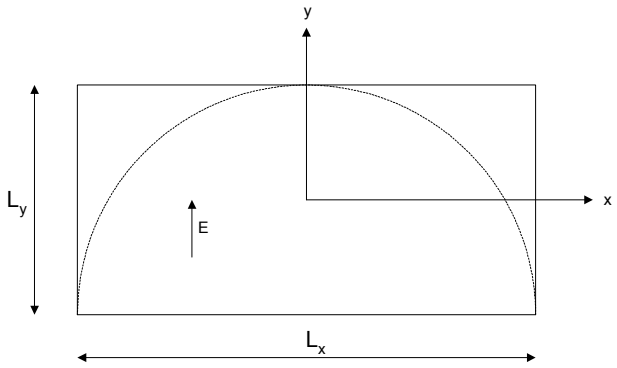

Figure 6. Horn aperture showing TE_{10} mode electric field distribution

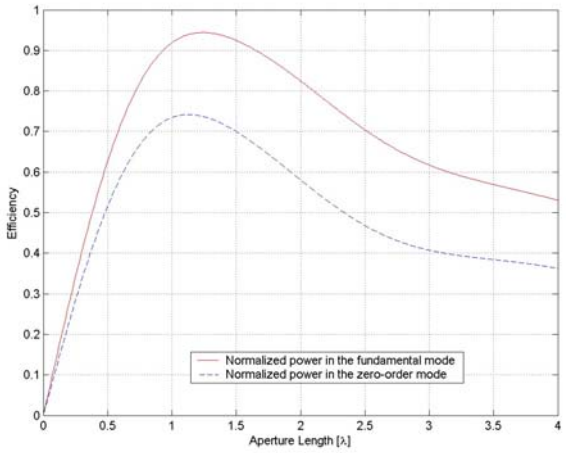

Figure 7. Efficiency of TE_{10} mode as a function of aperture dimensions.

electric field distribution present in the aperture is going to propagate to the receiver.

The feed antenna for the inflatable dish is a rectangular horn. At the X_L band carrier frequency only the TE_{10} mode will propagate in the WR-112 waveguide. Other modes may exist at the aperture of the feed horn, but these modes will become evanescent and will not propagate into the WR-112 to the LNA. The dish electric field distribution present in the aperture of the rectangular horn must be expanded in terms of the fundamental modes of the aperture. Only the power in the TE_{10} mode at the aperture will propagate through the WR-112 waveguide to the receiver. Figure 6 shows a diagram of the feed horn aperture and the TE_{10} mode distribution that will propagate to the LNA. The TE_{10} mode is described by a cosine distribution in the x-dimension and a uniform distribution in the y-dimension.

The modal expansion of the dish electric field distribution as a function of aperture length is expressed as

$$E(\xi) = \frac{A_0}{2} + \sum_{k=1}^{\infty} A_k \cos\left(\frac{k\pi}{L_\xi}\xi\right) \quad (4)$$

The mode amplitudes are expressed as

$$A_k = \frac{1}{L_\xi} \int_{-\frac{L_\xi}{2}}^{\frac{L_\xi}{2}} E(\xi)\cos\left(\frac{k\pi}{L_\xi}\xi\right) \quad (5)$$

The length of the waveguide in the x-dimension is calculated by maximizing the A_1 modal amplitude in (5) and the length of the waveguide in the y-dimension is determined by maximizing the A_0 modal amplitude also in (5). Figure 7 shows a plot of the relative power in the A_1 and A_0 modal coefficients. The optimum length of the aperture in the x-dimension is 1.24λ and the optimum width in the y-dimension is 1.13λ.

Custom pyramidal horns are expensive, so a standard gain pyramidal horn with aperture dimensions closest to the optimum dimensions was chosen. The standard gain horn closest to the optimum aperture dimension is the 15-dB standard gain horn. The dimensions of the 15-dB standard gain horn are 1.86λ in the x-dimension and 1.37λ in the y-dimension. Using the plot in Figure 7, the efficiency of the standard gain horn is horn approximately 2.0 dB. This is actually an under measurement of the horn efficiency because the TE_{10} mode is not the product of a uniform distribution and the cosine distribution, rather it is the vector combination of the two distributions. The above efficiency value is adjusted by 0.5 dB to account for the under measurement. The adjusted efficiency of the horn is =1.5 dB. This loss is equivalent to the spillover loss and the dish illumination efficiency combined.

B. Figure of Merit Calculation

The performance of the communication system that the dish will be demonstrated with is specified in terms of the receiver gain divided by the receiver noise temperature, commonly referred to as the figure of merit. The gain of the receiver system calculated in dB is expressed as

$$G_R = G_{dish} - \eta_{surface} - \eta_{blockage} - \eta_{feedhorn} - \eta_{polarization} + G_{LNA} - L_{cables} \quad (6)$$

Using the values shown in Table 1, the receiver gain is calculated to be $G_R = 101.0$ dB .

The receiver noise temperature is expressed as

$$T_R = T_{antenna} G_{LNA} G_{cable} + T_{LNA} G_{LNA} G_{cable} + T_{cable} G_{cable} \quad (7)$$

TABLE I

Receiver Gain Variables

Symbol	Description	Value [dB]
G_{dish}	Gain of the 4.8 m dish	51.5
$\eta_{surface}$	Surface roughness efficiency	0.5
$\eta_{blockage}$	Blockage efficiency	0.01
$\eta_{feedhorn}$	Feedhorn efficiency	1.58
$\eta_{polarization}$	Polarization efficiency	3.0
G_{LNA}	LNA Gain	66.0
L_{cable}	Cable Loss	11.0

TABLE II.

Receiver Noise Temperature Variables

Symbol	Description	Value
$T_{antenna}$	Blackbody radiation from cold sky	50 [K]
T_{LNA}	LNA noise temperature	60 [K]
T_{cable}	Cable noise temperature	290 [K]

Using the values shown in Table 2, the receiver noise temperature is calculated to be $T_R = 3.5\times10^7$ K = 75.4 dBK . The figure of merit is calculated to be 25.6 dB/K. This shows that the receiver comprised of the inflatable dish, LNA, and 25-foot coaxial cable will perform at least as well as the current receiver.

IV. SOLAR CALIBRATION

The inflatable dish antenna is constructed by integrating the radome, lenticular, and the RF feed structure. Figure 8 shows the dish during inflation and after inflation. Due to the nature of the integration, there is no way to guarantee that the focal point of the dish is exactly where it is designed to be. The only way to locate the true focal point of the dish is with measurements. Ideally, the gain pattern of the dish would be measured from a source mounted on a tall tower in the antenna far field. The far field of a 4.8-meter dish is 1.15 km. A test range that can handle antennas of this size was not available for testing, so the sun was used as an RF source.

A. Solar Power Calculations

To measure the noise power from the sun, a spectrum analyzer in a fixed-tune mode (zero span) is used to measure the time domain noise samples. It is assumed that the sun radiates uniformly over all microwave frequencies measured by the receiver. The solar flux density is used to calculate the noise power from the sun. An expression for the solar flux density of the sun is

a.

b.

Figure 8. a. Inflation of radome and lenticular with the inflation control system in the foreground. b. Fully inflated terrestrial based dish antenna.

$$F_{sun} = 3.6\times10^{-30}\cdot f\left[\frac{\mathrm{W}}{\mathrm{m}^2 Hz}\right] \tag{8}$$

The actual solar flux density of the sun is also measured and posted daily by NASA [4]. Equation (8) matches the daily measured results well, as expected. The noise power from the sun is calculated by multiplying the solar flux density by the aperture area of the 4.8-meter dish and by multiplying the result by receiver filter bandwidth. Noise measurements made using a spectrum analyzer produce a 2.0 dB under measurement because the analyzer averages in log space instead of linear space and because the equivalent noise bandwidth is not the same as the resolution bandwidth. The dish has an absolute area of 18.1 m^2, and assuming a 60% efficiency, the effective area is 10.86 m^2. The resulting noise power density from the sun at a frequency of 7.5 GHz in a dish with effective area 10.86 m^2 is $2.93\times10^{-19}\left[\frac{\mathrm{W}}{\mathrm{Hz}}\right]$. The 3 dB bandwidth of the LNA is 4 GHz. The noise power output from the LNA is calculated to be 3.5 dBm. The 1 dB compression point of the amplifier is 10 dBm, so the LNA is not saturated from the sun noise power. The resolution bandwidth of the spectrum analyzer is set to 1 MHz. The peak power expected from the sun in the 1 MHz bandwidth is

$$\begin{aligned} P_{sun\_peak} &= F_{sun} + 10\log\left(BW_{res}\right) + 10\log\left(A_{dish}\eta_{ap}\right) - L_{pol} \\ &\quad + G_{LNA} - L_{cable} + 2 \\ &= -41.5 \text{ dBm} \end{aligned}$$

where the 2 dB comes from the spectrum analyzer correction factor for noise calculations. The expected noise power when the dish is pointed at the cold sky is calculated as

$$\begin{aligned} P_{cold\_sky} &= 10\log\left(G_{LNA}k\begin{pmatrix} T_{ant}G_{LNA}G_{cable} \\ +T_{LNA}G_{LNA}G_{cable} \\ +T_{cable}G_{cable} \end{pmatrix} BW_{res}\right) + 2 \\ &= -59.6 \text{ dBm} \end{aligned} \tag{10}$$

The peak solar power and cold sky noise floor estimates will be used to compare to the measured values.

B. Solar Power Measurements

The sun is tracked optically using an equatorial mount test stand. An equatorial mount has two axes, and one of the axes can be aligned parallel to the Earth's axis. This allows tracking of celestial objects in one dimension only. As shown in Figure 8b, the inflatable dish is mounted in a bowl connected to the equatorial sun track test stand. Outriggers and non-conducting guy wires are used to further stabilize the dish from wind loading. A pinhole sun boresight scope, shown in Figure 9, is used to steer the antenna boresight of the dish in the direction of the sun. The pinhole sun boresight scope consists of two flat plates separated by 1 meter. The flat panel closest to the sun has a 3.175 mm diameter hole drilled through it and the flat panel furthest from the sun has a grid attached to it. The pinhole sun boresight scope is mounted to the side of the spherical radome. The sunlight passing through the 3.175 mm hole produces an image on the grid when the boresight of the dish in near the direction of the sun. The location of the grid is marked where the maximum power from the sun is measured. After time passes and the sun moves off of the antenna boresight, the equatorial test stand is adjusted so that the light through the 3.175 mm hole in the pinhole sun boresight scope is adjusted back to the marked location on the grid. The width of the sun at X_L band

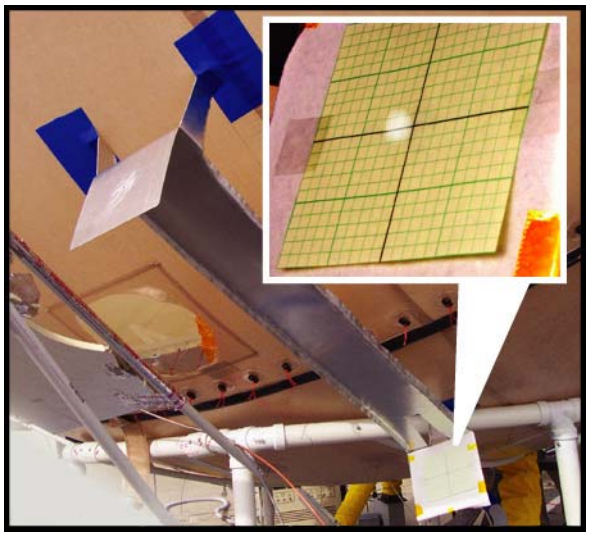

Figure 9. Pinhole sun boresight scope. Inset shows solar image on the scope grid.

is about 0.55 degrees. The 3dB beamwidth of the dish is calculated to be 0.49 degrees, so it is obvious that the sun tracker and sun locator must have a high degree of steering control accuracy and stability in order to accurately measure the sun. The test setup used in this experiment does not have the pointing accuracy and stability needed for attaining accurate power measurements from the sun, but it does provide a close estimate.

On February 24th, the dish was inflated outdoors and a solar gain measurement was recorded. After scanning the test stand in azimuth and elevation for a while, the dish was oriented toward the sun. It proved to be very difficult to find the 0.55 degree diameter sun using a 0.49 degree beam with the test stand used in this experiment. At 15:00 CST, a peak in the measured noise power, close to theoretical was measured. Figure 10 shows the results of letting the sun walk out of the main beam. The sharp rise at the beginning of the plot is where the direction of the sun is located with the narrow beam of the dish. The location of the sun on the grid of the pinhole sun boresight scope was marked. The oscillations following the sharp peak are adjustments made to the test stand to find the highest peak in measured power. Once the highest peak was measured, the test stand was locked into place and the power measurements of the sun walking out of the main beam were measured. The noise power measurements are time stamped by the data collection system. The sun travels 0.25 degrees every minute, so the time measurements in the data collection can be translated to angular movement of the sun. The abscissa of the plot in Figure 10 is expressed in degrees. The measured solar power gracefully degrades to the noise floor of the measurement device. The predicted noise floor, shown in Figure 10, is very close to the measured noise floor within 0.5 dB. The winds during this test were reported at 6-13 kph.

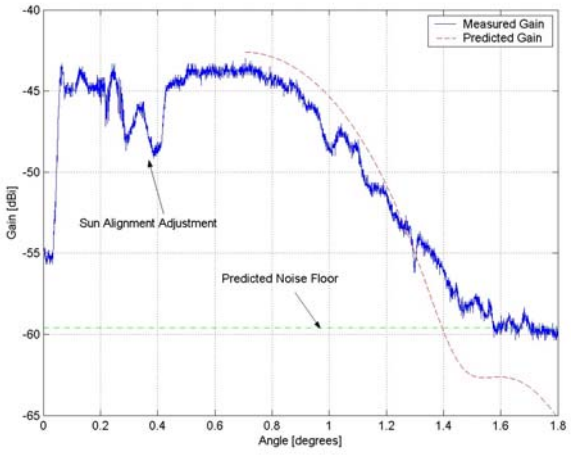

Figure 10. Measured gain from sun along with the predicted gain pattern and predicted measurement noise floor.

A comparison of the predicted antenna pattern and the measured antenna pattern is also shown in Figure 10. The peak of the predicted antenna pattern was shifted in angle space to the location of the peak measured power. The two plots have many observable differences. First of all, the measured peak is about 1.5 dB lower than the theoretical peak. It is conjectured that the low measured peak power comes from the fact that the dish was not truly boresight on the sun, the feed horn is not located at the true focal point of the dish, or, most likely, a combination of both of these errors. The predicted sun pattern is calculated by averaging the true antenna pattern of the dish by a sliding window the size of the angular size of the sun. The reason for averaging the dish pattern over the angular size of the sun is because the sun is not a point source relative to the beam width of this dish. Recall that the sun is roughly 0.55 degrees at X_L band and the 3dB beamwidth of the dish is only 0.49 degrees. Using the large sun, relative to the main beam of the dish, as an illumination source will have an averaging effect on the measured pattern of the dish. Averaging the ideal pattern over a 0.55-degree window results in the slope of the main beam is not be as sharp and the nulls are not as deep compared to the ideal pattern. Adjusting the feed horn location to match the phase center of the feed horn to the focal point of the dish may get the peak power closer to the predicted value, but with the tracking accuracy of the test equipment being used, the measured values in Figure 10 are probably as good as can be expected using the sun as an RF source.

V. CONCLUSIONS

A lightweight inflatable dish is presented as an alternative to the heavy, rigid dish antennas used for most terrestrial platforms. Using technologies that are common to space-based platforms, a much lighter dish with a much lower stowed volume is achievable. The reduction in weight and

the reduction in stowed volume are both an order of magnitude less than those of the conventional terrestrial counterpart. The inflatable dish is also cheaper to manufacture than a rigid dish.

Pattern measurements were made using the sun as an RF source. The pointing and tracking accuracy of the equatorial test stand used in the experiment were not accurate enough to truly boresight the dish in the direction of the sun. The low measured peak power is also a result of not having the phase center of the feed horn matched to the focal point of the dish. Given the limitation of the test equipment, measuring the antenna pattern of the dish to within 2 dB of the predicted value is acceptable.

The inflatable dish will be integrated with a fielded satellite communication system in late March. Using the dish in an operational data link will allow for the evaluation of the antenna's performance in different terrestrial weather environments.

ACKNOWLEDGMENT

We would like to thank the Assistant Secretary of Defense, Command, Control, Communications and Intelligence, The Pentagon, Wash D.C. for funding for this project. We would also like to thank Bill Clayton of SRS Technologies for all of his time designing and building the solar tracking test stand.

REFERENCES

[1] Pearson, J.C, Gierow, P.A., Lester, D.M., "Near term in-space demonstration of an inflatable concentrator," AIAA Paper 99-1073, Aerospace Sciences Meeting, Reno, NV. January 11-14,1999.

[2] John Huang, "The Development of Inflatable Array Antennas", *IEEE Antennas and Propagation Magazine*, vol 43, no. 4, August 2001, pp. 44-50.

[3] Robert Hoferer and Yahya Rahmat-Samii, "RF Characterization of an Inflatable Parabolic Torus Reflector Antenna for Space-Borne Applications," IEEE Trans. Antennas and Propagat. Vol 46, no 10, October 1998. pp 1449-1457.

[4] H. Fang et. al. "Development of a Three-Meter Ka-band Reflectarray Antenna," American Institute of Aeronautics and Astronautics, AIAA 2002-1706, pp 1-9.

[5] Bokulic, R. S., "Use Basic Concepts to Determine Antenna Noise Temperature," *Microwaves & RF*, March, 1991. pp 107-115.

[6] Sirmans, D. and Urell, B. "On Measuring WSR-88D Antenna Gain using Solar Flux," Next Generation Weather Radar Program. January 03, 2001.

[7] Love, A. W., "Some Highlights in Reflector Antenna Development," Radio Science, vol. 11, nos. 8, 9, August-September 1976.

[8] gopher://solar.sec.noaa.gov/00/lists/radio/rad